Journal of Ceramic Processing Research. Vol. 9, No. 4, pp. 421~424 (2008)

J O U R N A L O F
Ceramic Processing Research

Laser microfabrication of alumina-silicon carbide nanocomposites

Kwang-Ryul Kim[a], Jae-Hoon Kim[a], Kwang-Ho Kim[b], Koichi Niihara[c] and Young-Keun Jeong[b,*]

[a]*Department of Electronics and Computer Engineering, Hanyang University, Seoul 133-791, Korea*
[b]*National Core Research Center for Hybrid Materials Solution, Pusan National University, Busan 609-735, Korea*
[c]*Department of Electrical Engineering, Nagaoka University of Technology Niigata 940-2188, JAPAN*

Alumina-silicon carbide nanocomposites have many potential applications, because of their excellent mechanical properties. However, they are very difficult to fabricate for MEMS devices due to the difficulty in machining these nanocomposites. Alumina-silicon carbide nanocomposites sintered by a pressureless-sintering process have been fabricated using state-of-the-art laser microfabrication technology to find a way out of this difficulty. A femto-second laser with a specially equipped optical system was prepared and tested for nano and micro scale microfabrications of the material. The relationship between material ablation rate and energy fluence is theoretically investigated. In addition, the relationship is verified using cross-sectional SEM analysis of laser microfabricated alumina and alumina-silicon carbide samples. It is found that the nanocomposites are clearly fabricated using the femto-second laser and the surface roughness is acceptable for any MEMS parts.

Key words: Nanocomposite, Femto-second laser, Microfabrication.

Introduction

Since Niihara and coworkers [1-4] reported that the incorporation of nanometer-sized dispersoids into a ceramic matrix can significantly improve mechanical properties, there has been a growing interest in ceramic-matrix nanocomposites. Generally, these nanocomposites have been fabricated to high densities via hot pressing, because of the difficulty in densifying nanocomposites via conventional sintering. However, this process can produce only ceramic articles of simple geometrical shapes and would be expensive and unsuitable for mass production. For many potential applications of these materials, a pressureless-sintering process would be preferable if full density could be achieved. From this standpoint, we successfully fabricated alumina-silicon carbide nanocomposites using pressureless sintering and post-hot isostatic pressing (HIPing) [5].

Alumina-silicon carbide nanocomposites have many potential applications, because of their excellent mechanical properties. However, they are very difficult to fabricate for Micro-Electro-Mechanical Systems (MEMS) devices due to the difficulty in machining these nanocomposites. In this study, therefore, we have attempted to microfabricate nanocomposites using a femto-second laser. Materials research for metals and glasses using femto-second lasers has been investigated, but there are few studies reported for laser micromachining of crystalline ceramic materials [6-9].

*Corresponding author:
Tel : +82-51-510-2483
Fax: +82-51-518-3360
E-mail: nano@pusan.ac.kr

Analysis of the Ablation Depth & Evaporation Rates

A femto-second laser was prepared and installed with a special optical system for nanocomposites micromachining. The femto-second laser has very short pulse duration of 100 femto-seconds. Because the energy transfer time from electrons to ions by Coulomb collisions is significantly longer than this duration, the conventional hydrodynamics and thermal analysis theory can not be applied to analyze this ultra-short interaction [10]. Therefore, the mechanism of ablation of the nanocomposite by the femto-second laser will be described in an explicit analytical form. The threshold laser fluence for materials processing can be found out in the following theory. If the energy conservation law for the change in the electron energy or electron temperature due to absorption in the skin layer l_s is integrated over time and space, we obtain the following equation for the electron temperature [10]:

$$T_e = \frac{4}{3}\frac{AI_0 t}{l_s n_e}\exp\left\{-\frac{2z}{l_s}\right\}, \qquad T_e \approx \varepsilon_F \tag{1}$$

where, ε_F is the Fermi energy, A is the ratio of the absorption, I_0 is the incident laser intensity, t is the time, z is the depth from the surface, and n_e is the electron number density. The ablation threshold for the material is defined as the electron energy should be equal to the sum of the atomic bonding energy and the work function in a surface layer $d<<l_s$ by the end of the laser pulse. We obtain the energy condition for the ablation threshold using the above equations for the electron temperature:

$$\varepsilon_e = \varepsilon_b + J_i = \frac{4}{3}\frac{AI_0 t_p}{l_s n_e} \quad (2)$$

where, t_p is the laser pulse duration, ε_e is the electron kinetic energy, J_i is the ionization potential, and ε_b is the binding energy of the ions. Consequently, the laser threshold fluence for the ablation of the material is defined as follows:

$$F_{th}^{nanocomp} \equiv I_0 t_p = \frac{3}{4}(\varepsilon_b + J_i)\frac{l_s n_e}{A} \quad (3)$$

The ablation depth d_{ev} is of the order of the skin depth if we create a hole with the fluence near the ablation threshold of the femtosecond laser. Because of the exponential increase of the incident electric field and electron temperature in the material according to equation (1), it increases logarithmically with the laser fluence as follows:

$$d_{ev} = \frac{l_s}{2}\ln\frac{F}{F_{th}} \quad (4)$$

Defined as the number of particles evaporated per unit area per second, the average evaporation rate may be estimated using the energy conservation law for a femto-second laser matter interaction mode. Since the total absorbed femto-second laser energy flux in the ablation mode is balanced by the outflow of the ablated atoms times the energy expense per atoms which is equal to the Fermi energy, the ablation rate for the femto-second laser regime is expressed as [10]:

$$(nv)_{femto} \approx \frac{AI}{\varepsilon_F} \quad (5)$$

Experimental

Materials

The α-Al_2O_3 powder that was used in this study (TM-DAR, Taimei Chemicals Co., Nagano, Japan) had a purity of 99.99%, a mean particle size of 0.21 mm, and a specific surface area of 14.7 m^2/g (as reported by the manufacturer). β-SiC powder (Ibiden Co., Gifu, Japan) had a mean particle size of 0.27 μm (average grain size, by transmission electron microscopy (TEM), of 70 nm) and a specific surface area of 23.5 m^2/g. The combined powder (Al_2O_3-5 vol%SiC) was ball-milled in ethanol for 24 h using high-purity Al_2O_3 balls (5 mm in diameter) in a polyethylene pot. Then, soft agglomerates of the dried powders were crushed via dry ball-milling for 24 h using Al_2O_3 balls that were 10 mm in diameter.

The mixed powder was uniaxially pressed at 30 MPa into bars with dimensions of 5.5 mm × 6.4 mm × 53 mm and isostatically pressed at 200 MPa. The powder compacts were sintered in flowing argon at 1800 °C for 2 h. The subsequent HIP treatment was performed at 1600 °C for 1 h in an argon atmosphere of 150 MPa. After HIPing, the full

Laser Micromachining

A femto-second laser was prepared and installed with a special optical system for micromachining of the alumina-silicon carbide nanocomposites. The laser specifications are shown in table 1. Radiation from the femto-second laser goes through a shutter(SH), neutral density filter(ND) and aperture and the light is delivered using mirrors(M) and focused through a 20X objective lens. A beam splitter (BS) is used for a real-time CCD camera. The system configuration is presented in Fig. 1. We used a beam spot size of 8 μm for our tests.

Table 1. Femto-second laser specifications

Items	Specifications
Laser source	Ti:Sapphire
Wavelength	λ = 790 nm
Pulse Energy	3.5 mJ/kHz
Pulse Duration	100 fs
Beam Diameter	8 μm
Beam Quality	≤ 1.8
Beam Mode	TEM00 Gaussian

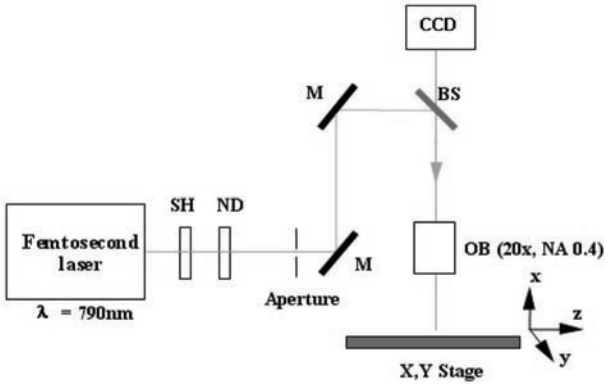

Fig. 1. System configuration for the femto-second laser.

Results

Cross-sectional view of the grooves which were microfabricated using the femto-second laser for the alumina and alumina-silicon carbide samples are shown in Fig. 2. The power densities from the left side are 0.91, 0.034, and 0.007 W respectively. It is obvious that the results form the alumina-silicon carbide presented better edge quality and machinability. The groove depth in the fused silica is generally 120 μm at 0. 91 W, but those of the above two materials are approximately 25 μm. Therefore, it is expected that micromachining for the crystalline materials requires more time than for the glass. The relationship between the ablation depth and laser fluence is plotted in Fig. 3. Comparing equation (4), the result for alumina increases logarithmically with the laser fluence. However, the result for the nanocomposite composed of alumina and silicon carbide does not follow this trend since the theoretical analysis is performed assuming properties for a single component material.

Figure 4(a) shows Al_2O_3 was inhomogeneously machined

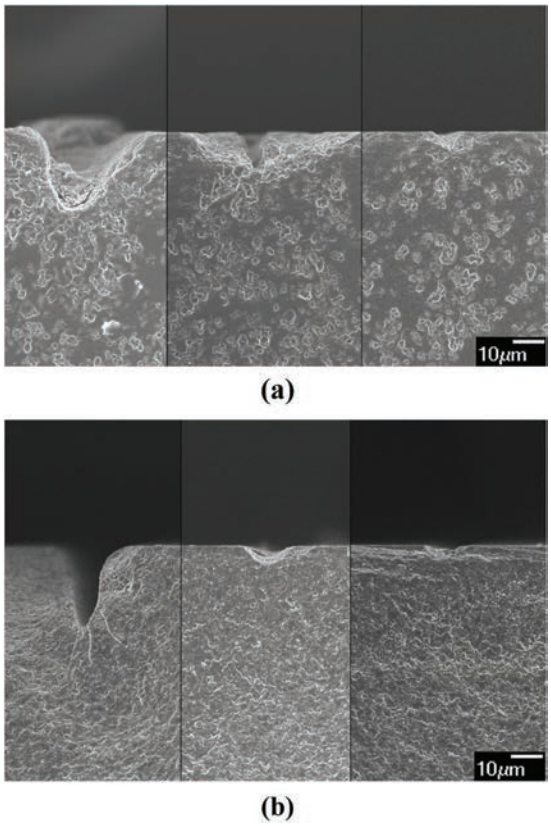

Fig. 2. SEM micrographs for cross sections of (a) Al_2O_3 and (b) Al_2O_3-SiC nanocomposite after an energy scan.

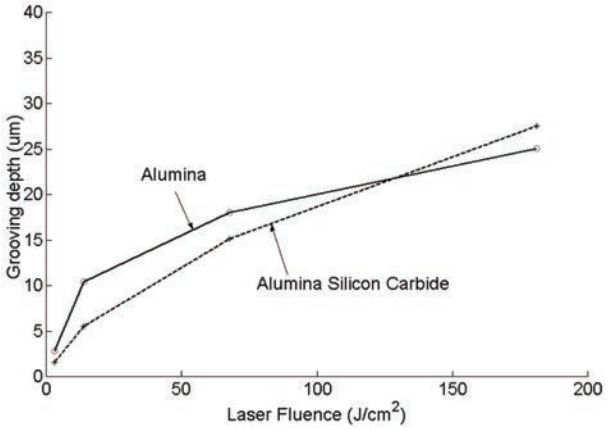

Fig. 3. Experimental results of the relationship between the ablation depth and laser fluence for the Al_2O_3 and Al_2O_3-SiC nanocomposite.

by the femto-second laser. This phenomenon can be explained by general keyhole dynamics. The evaporated material and plume of the Al_2O_3 rapidly moved forward and backward inside the keyhole, so the propagating laser beam is absorbed and blocked by them. The top picture of Fig. 4(a) shows that the surface of the alumina around the keyhole falls to pieces. It is considered that the low thermal shock resistance of alumina compared with that of the nanocomposite might be explaining this phenomenon [11].

In addition, the Fig. 4(b) shows a fairly good machining

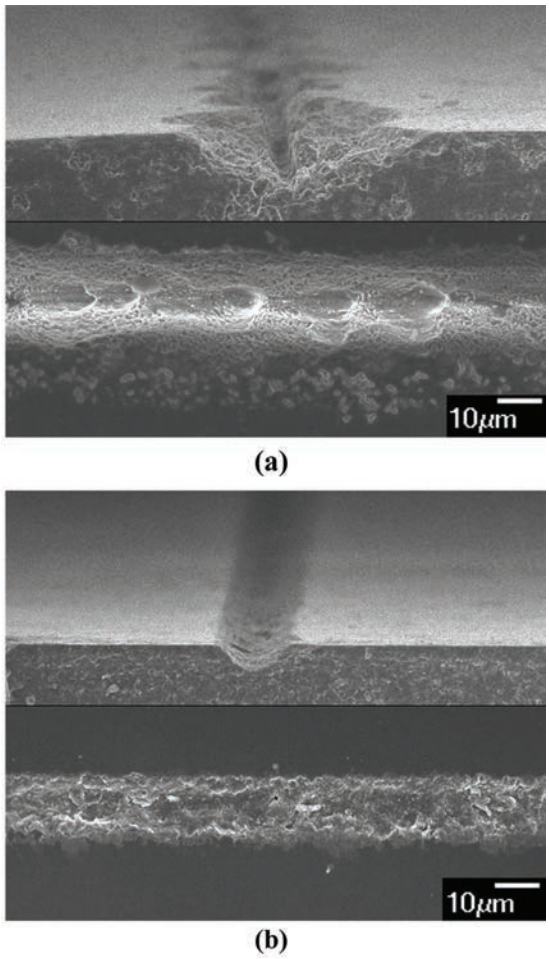

Fig. 4. SEM micrographs for (a) Al_2O_3 and (b) Al_2O_3-SiC nanocomposite after an energy scan (top: cross sectional view, bottom: top view).

Table 2. Properties of Al_2O_3 and Al_2O_3/SiC nanocomposites

	Al_2O_3	Al_2O_3/SiC
Grain size	8 μm	1.3 μm
Fracture strength at room temp.	620 MPa	1000 MPa
Fracture strength at 1000 °C	430 MPa	980 MPa

result for the alumina-silicon carbide nanocomposite. It is found that there is no microstructural damage by the laser energy as was shown in Al_2O_3. The good machinability of the alumina-silicon carbide nanocomposite results from the lower light transmittance since the laser energy is more absorbed in the gray-colored nanocomposite than in the white-colored alumina. In addition, the nanocomposite has a higher mechanical strength and a smaller grain size than those of Al_2O_3, as shown in table 2 [5].

A mechanical gear which had a diameter of 500 μm and a thickness of 100 μm was also micromachined for a MEMS micro part using femto-second laser, as shown in Fig. 5. It is found that the nanocomposite is successfully fabricated using the femto-second laser and the surface roughness is acceptable for any MEMS parts.

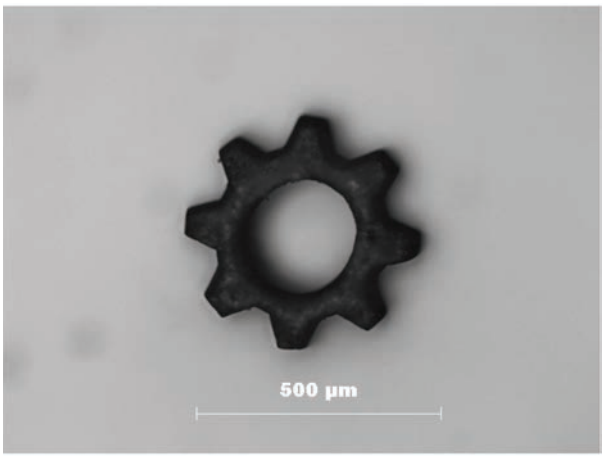

Fig. 5. A mechanical gear micromachined by the femto-second laser.

Conclusions

Alumina-silicon carbide nanocomposite sintered by a pressureless-sintering process has been fabricated using laser microfabrication technology. The relationship between material ablation rate and energy fluence was theoretically investigated. In addition, the relationship is verified using cross-sectional SEM analysis of laser microfabricated alumina and alumina-silicon carbide samples. The ablation depth of alumina increases logarithmically with the laser fluence. However, the result for a nanocomposite composed of alumina and silicon carbide does not follow their trend since the theoretical analysis was performed assuming properties for the single component material.

As expected, the nanocomposite showed a fairly good machining result and there was no microstructural damage by the laser energy. In addition, the nanocomposite was clearly fabricated using the femto-second laser due to its higher mechanical strength and smaller grain size as well as higher thermal resistance and lower light transmittance.

Acknowledgements

This study was supported by a grant from the National Core Research Center (NCRC) Program funded by KOSEF and MOST (R15-2006-022-01001-0).

References

1. K. Niihara and A. Nakahira, Proceedings of the Third International Symposium on Ceramic Materials and Components for Engines. 1998, pp. 919-926.
2. K. Niihara, A. Nakahira, G. Sasaki and M. Hirabayashi, Proceedings of the International Meeting on Advanced Materials, 1989, pp. 124-134.
3. K. Niihara and A. Nakahira, Advanced Structural Inorganic Composites. Edited by P. Vincenzini. (Elsevier Scientific Publishing, 1990) pp. 637-664.
4. K. Niihara, J. Ceram. Soc. Jpn., 99[10] (1991) 974-982.
5. Y.-K. Jeong, A. Nakahira and K. Niihara, J. Am. Ceram. Soc., 82[12] (1999) 3609-3612.
6. V.I. Kondrashov, L.A. Shitova, V.A. Litvinov and V.V. Surkov, Glass and Ceramics, 58[9-10] (2001) 303-305.
7. J. Cheng, M. Yen, C. Wei, Y. Chuang and T. Young, J. Micromech. Microeng., 15 (2005) 1147-1156.
8. H.Y. Zheng and T. Lee, J. Micromech. Microeng., 15 (2005) 2093-2097.
9. C.-H. Tsai and H.-W. Chen, Int. J. Adv. Manuf. Technol., 23 (2004) 342-349.
10. E.G. Gamaly, A.V. Rode, and B. Luther-Davies, Physics of plasmas, 9 (2002) 949-957.
11. S. Maensiri and S.G. Roberts, J. Am. Ceram. Soc., 85[8] (2002) 1971-1978.